Spiral and never-settling patterns in active systems

X. Yang,[1] D. Marenduzzo,[2] and M. C. Marchetti[3]
[1]*Physics Department, Syracuse University, Syracuse, New York 13244, USA*
[2]*SUPA, School of Physics and Astronomy, University of Edinburgh, Mayfield Road, Edinburgh EH93JZ, United Kingdom*
[3]*Physics Department and Syracuse Biomaterials Institute, Syracuse University, Syracuse, New York 13244, USA*
(Received 1 June 2013; published 17 January 2014)

We present a combined numerical and analytical study of pattern formation in an active system where particles align, possess a density-dependent motility, and are subject to a logistic reaction. The model can describe suspensions of reproducing bacteria, as well as polymerizing actomyosin gels *in vitro* or *in vivo*. In the disordered phase, we find that motility suppression and growth compete to yield stable or blinking patterns, which, when dense enough, acquire internal orientational ordering to give asters or spirals. We predict these may be observed within chemotactic aggregates in bacterial fluids. In the ordered phase, the reaction term leads to previously unobserved never-settling patterns which can provide a simple framework to understand the formation of motile and spiral patterns in intracellular actin systems.

DOI: 10.1103/PhysRevE.89.012711 PACS number(s): 87.18.Gh, 05.65.+b, 47.54.−r, 87.18.Hf

I. INTRODUCTION

Active systems, such as bacterial suspensions and cell extracts of cytoskeletal filaments and associated molecular motors, self-organize into a variety of intriguing patterns visible under the microscope [1–7]. *Escherichia coli* and *Salmonella typhimurium* colonies growing on soft agar, for instance, form crystalline or amorphous arrangements of high-density bacterial clumps [1–3], as well as stripes [8], while biofilms exhibit even more elaborate patterns [9]. In motility assays at high density, actin filaments self-organize into coherently moving structures such as clusters, swirls, and traveling bands [4,5]. The formation of plane and spiral actin waves has been predicted in models of actin cytoskeletal dynamics [10–12]. The organization of actin in clumps and spiral waves has also been reported *in vivo* in the actomyosin cytoskeleton of immobilized *Dictyostelium* cells [13,14]. The qualitative similarities between the patterns seen in these systems suggest that common principles may underlie such an organization. A large amount of theoretical work has been devoted to understanding the role of external chemical cues in driving pattern formation in active systems by modeling them via coupled nonlinear diffusion-reaction equations [1,14,15]. The model described here belongs, in contrast, to a new class of effective descriptions of active systems that can lead to pattern formation on the basis of a *minimal* set of physically motivated ingredients [16–18]. Specifically, cell reproduction and death in bacterial suspensions [19] or polymerization in actin gels and solutions [14] are described by a reactive logistic term. Also included are motility suppression due to cells crowding and cell alignment, as it may be induced by medium-mediated hydrodynamic interaction, biochemical signaling, and quorum sensing [8,20], or polarization of the actin cytoskeleton. The previous work summarized below has separately explored the role of some of the physical mechanisms included here but has not considered their combined effect. By proposing an effective model with no reference to specific biochemical signaling, we offer a unified minimal description of the emergence of complex structures in a variety of active systems; in particular, we here discuss the application of our theory to pattern formation in bacterial and actin systems.

II. CONTINUUM MODEL

Our model is formulated in terms of two continuum fields, the cell or actin filament density $\rho(\mathbf{r},t)$ and the polarization density $\mathbf{w}(\mathbf{r},t)$. The vector field $\mathbf{w}$ plays the dual role of an orientational order parameter describing the local polar alignment of active units traveling in the same direction and of current density. The continuum equations are

$$\partial_t \rho = -\nabla\cdot(v\mathbf{w} - D\nabla\rho) + \alpha\rho(1-\rho/\rho_s)\,, \tag{1a}$$

$$\partial_t \mathbf{w} + \frac{\gamma}{8\epsilon}\mathbf{w}\cdot\nabla(v\mathbf{w}) = -(\epsilon-\gamma\rho)\mathbf{w} - \frac{\gamma^2}{2\epsilon}|\mathbf{w}|^2\mathbf{w}, \\ -\frac{1}{2}\nabla\left(v\rho - \frac{3\gamma}{4\epsilon}vw^2\right) + D_w\nabla^2\mathbf{w}\,, \tag{1b}$$

where $v = v_0 e^{-\lambda\rho}$ is the density-dependent self-propulsion speed, with λ a parameter controlling the decay of motility with increasing density. The density equation is a convection-diffusion equation, augmented by the logistic term describing growth or decay at rate α, with a saturation density ρ_s. The polarization equation has the same structure as the well-known Toner-Tu model of flocking [21,22], but with additional nonlinearities arising from the density-dependent propulsion speed (for another generic equation of polar order in active systems see also [23]). It includes a convective term on the left-hand side, and active corrections to the effective pressure proportional to w^2. Here, ϵ is a rotational diffusion rate determined by the strength of rotational noise and γ is the strength of the alignment interaction. The diffusion coefficients D and D_w control gradients in the bacterial density and polarization. For simplicity we assume $D_w = D$. In the absence of the logistic reactive term, Eqs. (1) are a simplified version of those derived recently by coarse graining a Vicsek model with density-dependent self-propulsion speed [24]; the nonlinear advective terms which are here neglected do not change the physics (see Appendix D). In the following we measure times in units of ϵ^{-1} and lengths in units of v_0/ϵ. We also define dimensionless fields $\tilde{\rho} = \rho/\rho_s$ and $\tilde{\mathbf{w}} = \mathbf{w}/\rho_s$. The model

described by Eqs. (1) is then characterized by four dimensionless parameters, three of which are crucial to determine the physics: $\tilde{\lambda} = \lambda\rho_s$, $\tilde{\gamma} = \gamma\rho_s/\epsilon$, and $\tilde{\alpha} = \alpha/\epsilon$. These measure, respectively, the importance of density-dependent motility, of alignment, and of the reaction term. The fourth parameter, $\tilde{D} = D\epsilon/v_0^2$, denotes the scaled magnitude of the diffusion coefficient and elastic constant in the polarization equation.

When both motility suppression and the reaction term are neglected ($\tilde{\lambda} = \tilde{\alpha} = 0$), the equations describe the familiar Vicsek model. This has a mean-field transition from a homogeneous isotropic ($\mathbf{w} = 0$) state to a homogeneous polar (moving) state ($\mathbf{w} = w_0\hat{\mathbf{x}}$) when alignment $\gamma\rho_s$ exceeds noise ϵ ($\tilde{\gamma} > 1$). In this model emergent structures arise only in the polar state from the growth of fluctuations in the magnitude of polarization due to the $\gamma\rho_s$ term. Motility suppression qualitatively alters this well-known scenario. In models with density conservation ($\tilde{\alpha} = 0$) and no alignment ($\tilde{\gamma} = 0$), it can yield macroscopic phase separation, with large pretransitional density fluctuations, when $\tilde{\lambda} > 1$ [25,26]. Breaking density conservation is essential to yield the length selection seen in experiments, as shown in [18] for nonaligning systems, where a finite growth and/or death rate arrests phase separation, yielding concentric rings and high-density spots not unlike the bacterial "dots" observed in *Salmonella typhimurium*. The combined effect of alignment and motility suppression has only been considered in systems with density conservation ($\tilde{\gamma} \neq 0$, but $\tilde{\alpha} = 0$) [24]. In this case the interplay of self-trapping and alignment destabilizes both the homogeneous disordered and ordered states, yielding a rich collection of macroscopically separated traveling states, including bands, clumps, and lanes [24], but with no length selection. The minimal model proposed in this paper incorporates alignment, density growth or decay, and motility suppression and demonstrates that in different parameter regions these physical mechanisms can account qualitatively for the patterns seen in very diverse active systems. In particular, as we discuss more below, the patterns formed for small $\tilde{\alpha}$ are naturally associated with those seen in bacterial fluids, where growth is much slower than motion, whereas those observed for large $\tilde{\alpha}$ and $\tilde{\gamma}$ apply to polymerizing actin systems, where reaction rates vary depending on monomeric actin concentration, and the local density of actin fibers can promote their orientational order. In what follows, the language used to describe the dynamics in these parameter ranges will reflect that of the biophysical system they apply to.

III. EMERGENT PATTERNS IN THE ISOTROPIC STATE AND CHEMOTACTIC BACTERIAL DROPLETS

To examine the linear stability of the isotropic state for $\tilde{\gamma} < 1$, we study the dynamics of fluctuations $\delta\tilde{\rho} = \tilde{\rho} - 1$ and $\Theta = \boldsymbol{\nabla}\cdot\tilde{\mathbf{w}}$. For clarity of discussion, it is useful to restore dimension parameters. Working in Fourier space, we let $(\delta\tilde{\rho},\Theta) = \sum_{\mathbf{q}}(\rho_{\mathbf{q}},\Theta_{\mathbf{q}})e^{i\mathbf{q}\cdot\mathbf{r}}$. The time evolution of $\rho_{\mathbf{q}}$ and $\Theta_{\mathbf{q}}$ is then governed by

$$\partial_t\rho_{\mathbf{q}} = -v\Theta_{\mathbf{q}} - Dq^2\rho_{\mathbf{q}} - \alpha\rho_{\mathbf{q}}\,, \tag{2a}$$

$$\partial_t\Theta_{\mathbf{q}} = -\epsilon_r\Theta_{\mathbf{q}} + \tfrac{1}{2}(v + \rho_s v')q^2\rho_{\mathbf{q}} - Dq^2\Theta_{\mathbf{q}}\,, \tag{2b}$$

where $\epsilon_r = \epsilon - \gamma\rho_s$ is the rotational diffusion rate renormalized by alignment and the prime denotes a derivative with respect to density. The decay or growth of fluctuations is governed by the eigenvalues of Eqs. (2). The stability is controlled by the rate $s_+(q)$, given by

$$s_+(q) = -\frac{\alpha + \epsilon_r + 2Dq^2}{2} + \frac{\sqrt{(\alpha-\epsilon_r)^2 - 4\epsilon D_{sp}q^2}}{2}\,, \tag{3}$$

where we have introduced an effective diffusivity $D_{sp}(\rho) = (1 + \frac{1}{2}\frac{d}{d\rho})\frac{v^2(\rho)}{2\epsilon}$, with $v^2(\rho)/(2\epsilon)$ the diffusivity of a single particle performing a persistent random walk with run speed $v(\rho)$ and diffusion (tumble) rate ϵ. In Eq. (3) all quantities are evaluated at ρ_s. For the chosen form of $v(\rho)$, the effective diffusivity $D_{sp} = \frac{v_0^2}{2\epsilon}e^{-2\tilde{\lambda}}(1-\tilde{\lambda})$ can change sign when $\tilde{\lambda} > 1$. The rate s_+ becomes positive for $D_{sp} < -D(\sqrt{\frac{\alpha}{\epsilon}} + \sqrt{\frac{\epsilon_r}{\epsilon}})^2$. Motility suppression then promotes phase separation in regions of high and low density [25], which is in turn arrested by the density growth or decay. Active particles (here representing bacteria) tend to grow in low-density regions and die or decay in high-density regions; hence they must migrate from high-density to low-density regions to obtain a steady state. The interplay of these two mechanisms ultimately yields a stable pattern. The linear stability analysis also yields the wave vector $q_c \sim D^{-1/2}[\alpha\epsilon_r]^{1/4}$ of the most unstable mode: the length scale q_c^{-1} decreases with increasing α and ϵ_r, consistent with the behavior shown in the density maps of Fig. 1. For very large $\tilde{\lambda}$ the active contribution to the effective diffusivity vanishes as $D_{sp} \to 0$, and the homogeneous state is again stable. The "knee" in the curves at $\tilde{\lambda} = 1.5$ corresponds to the minimum of D_{sp} (Fig. 2). Finally, the instability exists even for $\alpha = 0$, although in this case the system coarsens into macroscopic phase separated regions, rather than forming a stable pattern (see Supplementary Movies 6 and 7) [34]. Increasing α for fixed alignment strength tends to stabilize the uniform state. Finally, Fig. 3 shows the patterns obtained from the spreading of a bacterial drop inoculated at the center of the sample.

In bacteria the birth and death rate α is of the order of inverse hours and the run length v_0/ϵ is typically $\sim 10 - 30\ \mu$m, with $\epsilon \sim 1\ \text{s}^{-1}$. In this case, and provided $\gamma\rho_s < \epsilon$, the dynamics of the polarization is much faster that of the density. One can exploit this separation of time scales by neglecting $\partial_t\mathbf{w}$ in Eq. (1b) and eliminating polarization in terms of density in Eq. (1a). At large length scales, this yields an effective diffusion equation of the type studied in [18], with a diffusivity that changes sign, signaling the onset of phase separation. In this range of parameters, incorporating polarization dynamics yields polar structure within the high-density static dots found in [18], with the dots turning into asters and spirals, but does not change the structure of the overall pattern. The polar structure of the dots shown in Fig. 1 arises when the density $\rho > \rho_s$ inside an individual dot is large enough that $\gamma\rho > \epsilon$, i.e., the system acquires polar order. To our knowledge, such static asters and spirals have not yet been reported in bacterial suspension, but they should be visible by electron microscopy in experiments with self-chemotactic bacterial strains in semisolid agar [27], as the density in the

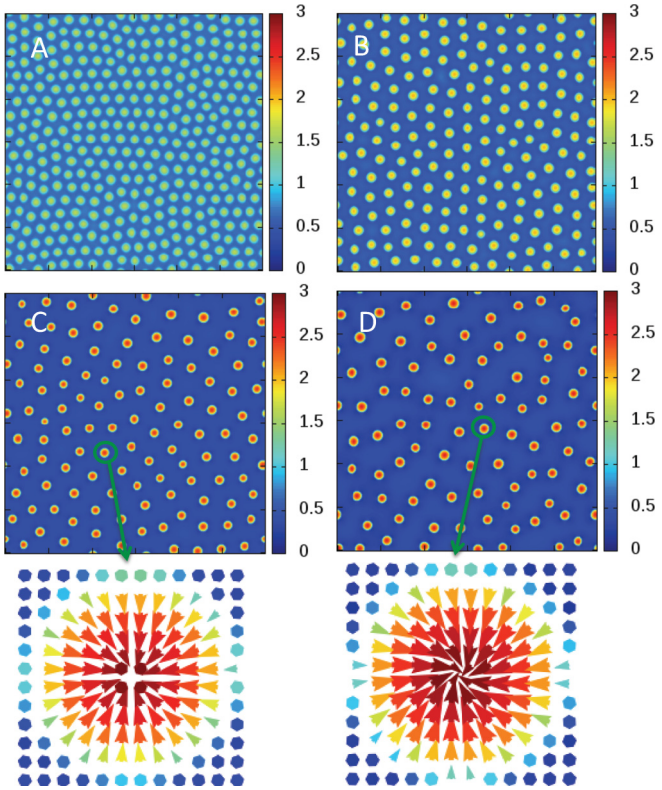

FIG. 1. (Color online) Color maps of the density obtained by numerical integration of Eqs. (1) in a box with periodic boundary conditions and an initial isotropic state ($\mathbf{w} = 0$) of uniform mean density $\rho_0 = \rho_s$, with small random fluctuations. The color bars give the values of the local density $\tilde{\rho} = \rho/\rho_s$. All images are for $\tilde{\lambda} = 1.4$, $\tilde{D} = 0.01$, $\tilde{\alpha} = 0.083$ and (from A to D) $\tilde{\gamma} = 0.50, 0.58, 0.75, 0.95$. The high-density static bacterial dots in A and B have zero or very small local polar order, as in [18]. In C and D polar order builds up in each dot, as highlighted by the blowups of individual dots shown in the bottom row. Here the polarization is displayed as an arrow of length proportional to its magnitude. The color refers to the density, with the same color scheme as indicated in the side bars (see also Supplementary Movies 1 and 2) [34].

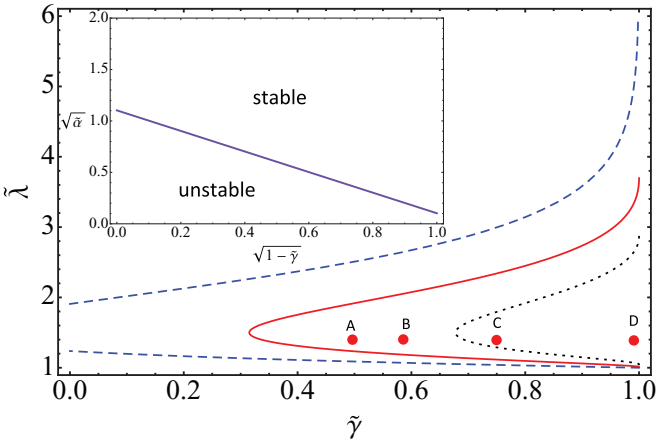

FIG. 2. (Color online) The boundary of linear stability of the homogeneous state ($\tilde{\gamma} < 1$) in the $(\tilde{\lambda}, \tilde{\gamma})$ plane for $\tilde{\alpha} = 0$ (dashed curve, blue online), $\tilde{\alpha} = 0.083$ (solid curve, red online), and $\tilde{\alpha} = 0.30$ (dotted curve, black online). The homogeneous state is unstable in the region to the right of each curve, up to the vertical axis $\tilde{\gamma} = 1$. The calculation is described in Appendix B. The dots labeled A, B, C, D show the location in parameter space of the images shown in Fig. 1 and refer to $\alpha = 0.083$. For a fixed value of $\tilde{\alpha}$, the region of $\tilde{\lambda}$ where the system is unstable grows as alignment increases. Conversely, increasing the birth or death rate for fixed $\tilde{\gamma}$ stabilizes the homogeneous state. This is highlighted in the inset that shows the linear stability boundary in the $(\tilde{\alpha}, \tilde{\gamma})$ plane for $\tilde{\lambda} = 1.4$. Note that in the inset the horizontal axis is $\sqrt{1-\tilde{\gamma}}$, i.e., alignment increases to the left.

resulting clusters has been estimated to be 100 times larger than in uniform cultures [28]. As $\tilde{\gamma} = \gamma\rho_s/\epsilon \to 1^-$, the polar structure becomes more pronounced. When all nonlinearities are taken into account (see Appendix D), close to the transition and for a large value of the reproduction rate, the model yields "blinking" dot patterns (see Supplementary Movie 5 [34]).

IV. EMERGENT PATTERNS IN THE POLARIZED STATE AND INTRACELLULAR ACTIN SYSTEMS

In the uniform polar state ($\mathbf{w} = w_0\hat{\mathbf{x}}$), instabilities exist even for $\lambda = 0$ and $\alpha = 0$ and these have been studied before [29,30]. The reactive logistic term provides a mechanism for pattern scale selection. The study of the dynamics in the polarized state for variable values of $\tilde{\alpha}$ may not apply to usual bacterial suspensions, where growth is slow with respect to motion, and aligning effects are insufficient to yield an overall orientationally ordered phase (one exception might be provided by swarms). This study is, however, highly relevant to actomyosin systems, where (i) immobilized motors (*in vitro*, e.g., in motility assays [4]) or treadmilling (*in vivo*) lead to propulsion; (ii) steric effects may cause motility suppression; (iii) polymerization (limited by actin crowding) occurs on time scales comparable to rotational diffusion, and (iv) the density can easily become large enough to induce local polar order [4].

For the parameters used in our model, when $\lambda = \alpha = 0$ fluctuations in the magnitude of polarization of wave vector $\mathbf{q} \| x$ destabilize the uniform state for $1 \leqslant \tilde{\gamma} \leqslant \frac{v_0}{4}\sqrt{\frac{\epsilon}{D}}$, while splay fluctuations with $\mathbf{q} \perp x$ are always unstable. Both these

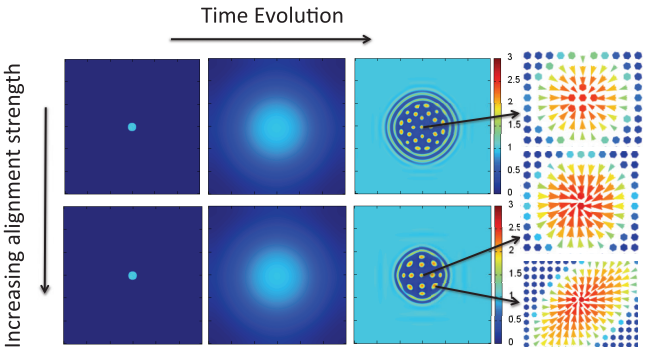

FIG. 3. (Color online) Snapshots of the spreading of a droplet inoculated at the center of the simulation sample for $\tilde{\gamma} = 0.83$ (top row) and $\tilde{\gamma} = 0.98$ (bottom row), with $\tilde{\alpha} = 0.167$, $\tilde{\lambda} = 1.40$, and $\tilde{D} = 0.01$. The simulation times are 1, 4000, 22 000 and 1, 4000, 14 000 from left to right, respectively, in units of ϵ^{-1}. The blowups to the right show the internal structure of the dots, as described in the caption of Fig. 1.

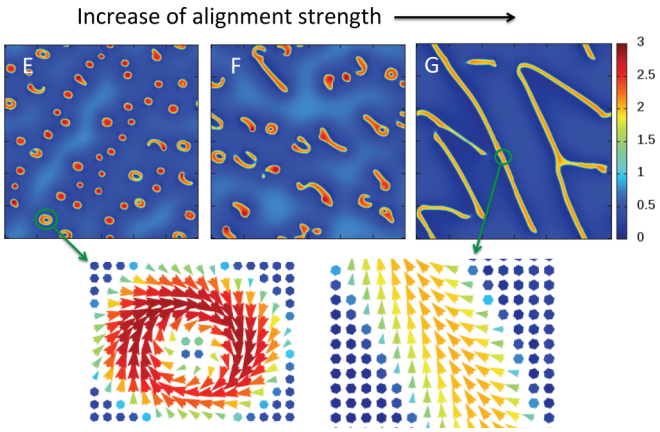

FIG. 4. (Color online) Patterns in the polar state obtained from a uniform initial state with small random fluctuations around $\tilde{\rho} = 1$ and $\tilde{\mathbf{w}} = \mathbf{0}$ for $\tilde{\alpha} = 0.08$, $\tilde{D} = 0.01$, and $\tilde{\lambda} = 1.10$. Rings and lanes emerge in (E), (F), (G) at $\tilde{\gamma} = 1.11, 1.25, 2.00$, respectively. We stress that the net total polarization of the lanes shown in frame G is directed at an angle to the long direction of the lanes, resulting in a transverse drifting motion (See Supplementary Movie 4) [34].

longitudinal and transverse instabilities have been discussed extensively. In particular, the longitudinal instability has been argued to signal the onset of high-density ordered bands normal to the direction of mean polarization traveling in a disordered low-density background [29,30]. The suppression of motility induced by a finite λ yields a host of complex structures, including traveling dots, stripes, and lanes that coarsen at long times into anisotropic phase separated states [24]. A finite value of $\tilde{\alpha}$ arrests the phase separation and yields patterns with a characteristic length scale, as shown in Fig. 4. In the region $\tilde{\gamma} > 1$ the patterns are always dynamical, with the spirals rings continuously breaking up and reconnecting, as displayed in Supplementary Movies 3 and 4 [34]. Such never-settling states are, interestingly, virtually absent (except for simple traveling waves) in previous versions of the model, neglecting either alignment or reaction.

The dynamical patterns featuring ever-evolving spirals and lanes in Fig. 4 bear a striking qualitative similarity to the actin waves and dynamical spiral patterns observed in the cytoskeleton of Dictyostelium [14,31]. In this system polymerization/depolymerization rates are of order 1–100 s^{-1}, and hence are comparable to the rotational diffusions rates $\epsilon \sim$ 1–20 s^{-1} for a 1-μm filament [32]. Here individual cells were first immobilized by depolymerizing actin with latrunculin. Upon latrunculin reduction, static spots of actin were seen to form in the cortex. At later times, the spots become dynamical and eventually turn into spiral waves that closely resemble our ever-evolving rings, and allow the cell to eventually resume motility. The experimental observation was modeled in [14] by a reaction-diffusion model where actin density and orientation growth are controlled by a chemical inhibitor. Our model provides a simpler physical interpretation of the self-organization, where chemical signaling does not need to be explicitly incorporated in the dynamics but only enters through effective parameters: λ that captures the aggregation of actin driven by membrane-bound protein complexes [31], and α representing the (crowding-limited) actin polymerization rate. The transition from actin clusters to spirals and finally to traveling waves, as observed in Supplementary Movies 1 and 4 of Ref. [31], is obtained in our model by increasing $\tilde{\gamma}$, as shown in Fig. 4 (see also Supplementary Movies 3 and 4) [34], which corresponds to increased alignment of the actin filaments *in vivo* due to the increase of density through polymerization.

V. DISCUSSION

In summary, we have studied an active system where constituents (i) align, (ii) move at a density-dependent speed, and (iii) reproduce, or undergo a logistic reaction. The first system this case refers to is that of a bacterial suspension. While it had been demonstrated before that the interplay of motility suppression and bacterial growth or death can yield stable structures in a simple effective model even in the absence of chemotaxis, our work shows that alignment interactions play a major role in pattern selection. When alignment is small ($\tilde{\gamma} \ll 1$), polarization decays on the time scale of the inverse rotational diffusion rate ϵ, that in bacteria is much faster than reproduction. Bacterial organization is then controlled by the dynamics of the density and results in patterns of high-density dots, depending on the initial conditions, as seen before. Alignment yields polar structure of increasing complexity (asters and spirals) within each dot, even for mean densities ρ_s below the value ϵ/γ required for the onset of mean-field polar order. Above the mean-field transition to a polar state ($\tilde{\gamma} > 1$) the patterns become dynamical, with ever-evolving rings and spirals that have not been obtained before in simple effective models. These latter structures closely resemble the actin spirals that have been observed *in vivo* in the cytoskeleton of Dictyostelium [31]. Finally, we note that evolving spiral patterns have also been obtained recently in a chemotactic model of swimmers [33].

ACKNOWLEDGMENTS

M.C.M. and X.Y. were supported by the National Science Foundation through Awards No. DMR-1004789, No. DMR-1305184, and No. DGE-1068780.

APPENDIX A: HOMOGENEOUS STATIONARY STATES

The continuum equations for the density $\rho(\mathbf{r},t)$ and polarization density $\mathbf{w}(\mathbf{r},t)$ given in Eqs. (1) of this article have two homogeneous, stationary solutions:

(1) a homogeneous isotropic state, with $\rho = \rho_s$ and $\mathbf{w} = 0$, for $\gamma\rho < \epsilon$ ($\tilde{\gamma} < 1$);

(2) a uniform polarized state, with $\rho = \rho_s$ and $\mathbf{w} \neq 0$ for $\gamma\rho > \epsilon$ ($\tilde{\gamma} > 1$).

Choosing the x axis along the direction of mean polarization, we find $\mathbf{w} = \hat{\mathbf{x}} w_0$, with $w_0 = \sqrt{2\epsilon(\gamma\rho_s - \epsilon)}/\gamma$, in the polarized state, which is also a uniformly moving state. Next we examine the linear stability of each of these two states with respect to small fluctuations in both fields from their uniform values. Quantities with a tilde above them are dimensionless, as defined in the main text.

APPENDIX B: LINEAR STABILITY OF THE ISOTROPIC STATE

We consider the dynamics of fluctuations $\delta\tilde{\rho}(\mathbf{r},t) = \tilde{\rho}(\mathbf{r},t) - 1$ and $\delta\tilde{\mathbf{w}}(\mathbf{r},t) = \tilde{\mathbf{w}}(\mathbf{r},t)$ to linear order. We let $\Theta = \boldsymbol{\nabla}\cdot\delta\tilde{\mathbf{w}}$ and denote by $\delta\tilde{\mathbf{w}}^{\perp}$ the transverse part of the polarization. The linearized equations for the fluctuations are then given by

$$\partial_t\delta\tilde{\rho} = -v\Theta + D\nabla^2\delta\tilde{\rho} - \alpha\delta\tilde{\rho}\,, \tag{B1a}$$

$$\partial_t\Theta = -\epsilon_r\Theta - \tfrac{1}{2}(v+\rho_s v')\nabla^2\delta\tilde{\rho} + D\nabla^2\Theta\,, \tag{B1b}$$

$$\partial_t\delta\tilde{\mathbf{w}}^{\perp} = -\epsilon_r\delta\tilde{\mathbf{w}}^{\perp} + D\nabla^2\delta\tilde{\mathbf{w}}^{\perp}\,, \tag{B1c}$$

where $\epsilon_r = \epsilon - \gamma\rho_s > 0$, $v = v_0 e^{-\tilde{\lambda}}$, and $\rho_s v' = -\tilde{\lambda}v_0 e^{-\tilde{\lambda}}$. The transverse part of the polarization is decoupled to linear order and always decays. It will be ignored in the rest of this section. Working in Fourier space, we let $(\delta\tilde{\rho},\Theta) = \Sigma_{\boldsymbol{q}}(\rho_{\boldsymbol{q}},\Theta_{\boldsymbol{q}})e^{i\boldsymbol{q}\cdot\boldsymbol{r}}$. The time evolution of the Fourier amplitudes $\rho_{\boldsymbol{q}}$ and $\Theta_{\boldsymbol{q}}$ is then governed by the equations

$$\partial_t\rho_{\boldsymbol{q}} = -v\Theta_{\boldsymbol{q}} - Dq^2\rho_{\boldsymbol{q}} - \alpha\rho_{\boldsymbol{q}}\,, \tag{B2a}$$

$$\partial_t\Theta_{\boldsymbol{q}} = -\epsilon_r\Theta_{\boldsymbol{q}} + \tfrac{1}{2}(v+\rho_s v')q^2\rho_{\boldsymbol{q}} - Dq^2\Theta_{\boldsymbol{q}}\,. \tag{B2b}$$

We seek a solution of the form $\rho_{\boldsymbol{q}},\Theta_{\boldsymbol{q}} \sim e^{s(q)t}$. The eigenvalues are then given by

$$s_{\pm}(q) = -\tfrac{1}{2}(\alpha+\epsilon_r+2Dq^2) \pm \tfrac{1}{2}\sqrt{(\alpha-\epsilon_r)^2 - 4\epsilon\mathcal{D}_{sp}q^2}\,, \tag{B3}$$

where we have introduced the effective diffusivity

$$\mathcal{D}_{sp} = \left(1+\frac{\rho}{2}\frac{d}{d\rho}\right)D_s = \frac{v_0^2}{2\epsilon}e^{-2\tilde{\lambda}}(1-\tilde{\lambda})\,, \tag{B4}$$

with $D_s = v^2/(2\epsilon)$. The diffusivity $\mathcal{D}_{sp}$ is negative for $\tilde{\lambda} > 1$ and has a negative minimum value at $\tilde{\lambda} = 1.5$. For $\tilde{\lambda} > 1.5$ it approaches zero from below. The eigenvalues $s_{\pm}(q)$ describe the time evolution of linear combinations of fluctuations in the density and the longitudinal part of the polarization density, which to linear order is proportional to the magnitude of the polarization field. When $\alpha = 0$, the mode $s_+(q)$ is hydrodynamic as $\mathrm{Re}[s_+(q\to 0)] = 0$, as required by density conservation, and describes the decay of density fluctuations. The mode $s_-(q)$ mainly describes the dynamics of polarization, which decays at a finite rate ϵ_r when $q = 0$ and becomes long lived at the transition where $\epsilon_r = 0$. This is highlighted by expanding the dispersion relations for small q, with the result

$$s_+(q,\alpha=0) = -q^2\left(D + \mathcal{D}_{sp}\frac{\epsilon}{\epsilon_r}\right) + O(q^4)\,, \tag{B5a}$$

$$s_-(q,\alpha=0) = -\epsilon_r - q^2\left(D - \mathcal{D}_{sp}\frac{\epsilon}{\epsilon_r}\right) + O(q^4)\,, \tag{B5b}$$

where the expansion can be carried out only away from the transition, where ϵ_r remains finite. When α is finite both modes are nonhydrodynamic. The s_+ mode is unstable when $\mathrm{Re}[s_+] > 0$, which gives the instability condition

$$\mathcal{D}_{sp} < \mathcal{D}_{sp}^c = -D\left(\sqrt{\frac{\alpha}{\epsilon}} + \sqrt{\frac{\epsilon_r}{\epsilon}}\right)^2 < 0\,. \tag{B6}$$

The linear stability boundary $\mathcal{D}_{sp}^c$ defined by Eq. (B6) is shown in Fig. 2 of the paper for $v = v_0 e^{-\tilde{\lambda}}$. Clearly the specific form of the stability boundary depends on the form chosen for $v(\rho)$. At large λ the diffusivity $\mathcal{D}_{sp}$ vanishes and the uniform state is stable, as obtained in Ref. [18]. As γ is increased for a fixed α, the region of instability widens. The instability occurs even for $\alpha = 0$, where $\mathcal{D}_{sp}^c = -D\frac{\epsilon}{\epsilon_r}$. In this case, however, the uniform state is unstable on all scales, corresponding to macroscopic phase separation [25], as shown in Fig. 6. The dispersion relation of the mode $s_+(q)$ is shown in Fig. 5 for various values of the alignment strength. The instability occurs in a band of wave vectors $q_1 < q < q_2$, with

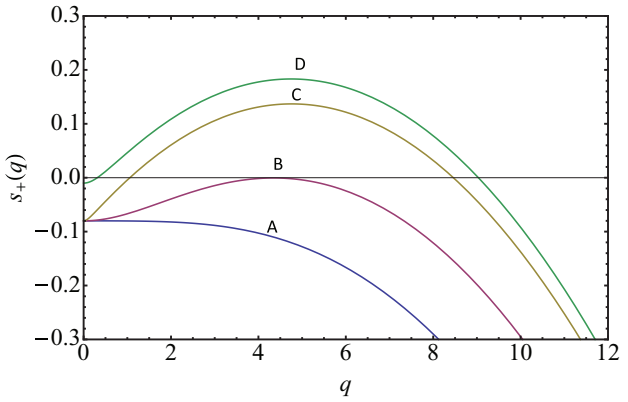

FIG. 5. (Color online) The dispersion relation of the mode $s_+(q)$ is plotted as a function of the wave vector q for $\tilde{\alpha} = 0.08$, $\tilde{D} = 0.01$, and $\tilde{\lambda} = 1.2$. The curves from A to D correspond to $\tilde{\gamma} = 0, 0.55, 0.9$, and 0.99. The homogeneous isotropic state is unstable for $s_+(q) > 0$ and stable for $s_+(q) < 0$. The instability is enhanced upon increasing the alignment strength $\tilde{\gamma}$ due to the decrease of the decay rate ϵ_r of the polarization as the mean-field transition at $\tilde{\gamma} = 1$ is approached from below. The instability exists in a band of wave vectors $q_1 < q < q_2$. When $\alpha < \epsilon_r$, as in typical bacterial suspensions, the decay rate at zero wave vector is controlled by α (curves A to C), while when $\alpha > \epsilon_r$, it is controlled by ϵ_r (curve D).

$$q_{1,2} = \sqrt{\frac{1}{2D^2}\{-[\mathcal{D}_{sp}\epsilon + D(\alpha+\epsilon_r)] \mp \sqrt{[\mathcal{D}_{sp}\epsilon + D(\alpha+\epsilon_r)]^2 - 4D^2\alpha\epsilon_r}\}}. \tag{B7}$$

When $\alpha = 0$, $q_1 = 0$ and $q_2 = \sqrt{-(\mathcal{D}_{sp}\epsilon + \epsilon_r D)}/D$. Conversely, at the mean-field transition where $\epsilon_r = 0$, $\mathcal{D}_{sp}^c = -D\alpha/\epsilon$ and we find $q_1 = 0$, $q_2 = \sqrt{-(\mathcal{D}_{sp}\epsilon + \alpha D)}/D$. To examine the behavior as the mean-field order-disorder transition is approached

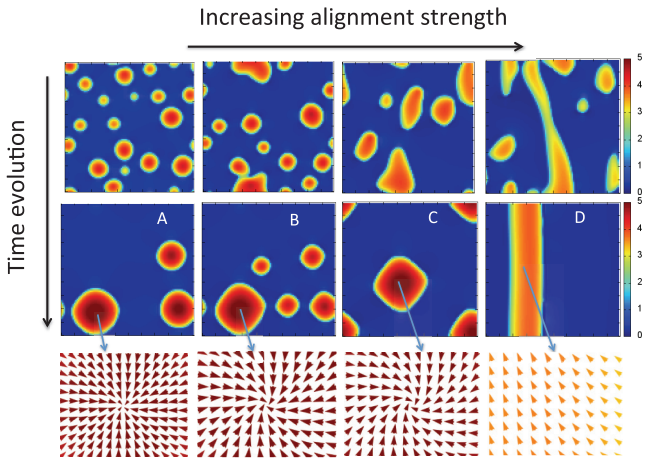

FIG. 6. (Color online) Density heat maps for $\tilde{D} = 0.01, \tilde{\lambda} = 1.2$, and $\tilde{\alpha} = 0$ showing macroscopic phase separation. The color scale is indicated to the right, and the values refer to $\tilde{\rho} = \rho/\rho_s$. From A to D, $\tilde{\gamma} = 0.50, 0.75, 0.96$, and 1.11. The time evolution shows the coarsening of the structures into a single large cluster. Upon increasing the alignment strength, the cluster starts to display polar order, as highlighted in the blowups in the bottom row showing maps of the polarization field.

from below, we let $\mathcal{D}_{sp} = \mathcal{D}_{sp}^c - \delta$, with $\delta > 0$. To leading order in δ we obtain

$$q_{1,2} \simeq \frac{(\alpha\epsilon_r)^{1/4}}{D^{1/2}}\left[1 \mp \frac{\delta^{1/2}}{2}\left(\frac{\epsilon}{D\sqrt{\alpha\epsilon_r}}\right)^{1/2} + O(\delta)\right]. \quad \text{(B8)}$$

At the onset of the instability, where $\delta = 0$, the wave vector of the unstable mode is $q_c = q_1 = q_2$, with

$$q_c = \frac{(\alpha\epsilon_r)^{1/4}}{D^{1/2}} . \quad \text{(B9)}$$

The wavelength of the pattern then scales as $\ell_c \sim q_c^{-1} = D^{1/2}(\alpha\epsilon_r)^{-1/4}$. Finally, when $D = 0$, the isotropic state is unstable for $\mathcal{D}_{sp} < 0$, i.e., $\tilde{\lambda} > 1$ and $q > \sqrt{\frac{\alpha\epsilon_r}{|\mathcal{D}_{sp}\epsilon|}}$. In other words, a finite value of D is needed to stabilize the system at small scales.

To make contact with the model of bacterial suspensions studied in Ref. [18] that neglect polarization, we assume $\alpha \ll \epsilon$, which is generally true for bacteria, and let $\tilde{\gamma} = 0$. In this case the fluctuations in polarization decay at the fast rate ϵ. On times large compared to ϵ^{-1}, we can neglect the time derivative on the left-hand side of Eq. (B2b), solve for $\Theta_{\mathbf{q}}$ to low order in $\mathbf{q}$, and eliminate the polarization from Eq. (B2a) to obtain a closed equation for the density, given by

$$\partial_t \rho_{\mathbf{q}} = -(D + \mathcal{D}_{sp})q^2\rho_{\mathbf{q}} - \alpha\rho_{\mathbf{q}} + \frac{D\mathcal{D}_{sp}}{\epsilon}q^4\rho_{\mathbf{q}} . \quad \text{(B10)}$$

In the region $\tilde{\lambda} > 1$ where $\mathcal{D}_{sp} < 0$, we can define an effective surface tension $\kappa_{\text{eff}} = D|\mathcal{D}_{sp}|/\epsilon$ and Eq. (B10) is then formally identical to the linearized form of the density equation proposed in Ref. [18]. This effective surface tension vanishes, however, at large λ, when $\mathcal{D}_{sp} \to 0$. In this limit the approximation used to obtain Eq. (B10) no longer applies.

Finally, we summarize a few key points:

(1) As discussed by Cates *et al.* [18], pattern formation in the isotropic state is the result of the interplay of motility suppression that drives the effective diffusivity $\mathcal{D}_{sp}$ negative triggering macroscopic phase separation, and birth or death, which arrests phase separation.

(2) Deep in the isotropic state ($\tilde{\gamma} \ll 1$), the polarization decays on microscopic times $\sim(\epsilon - \gamma\rho_s)^{-1} \sim \epsilon^{-1}$ and can be neglected. The instability is then controlled entirely by the dynamics of density fluctuations, as in the model of Ref. [18].

(3) When $\tilde{\gamma}$ approaches 1 from below, the decay of polarization fluctuations slows down. In this case if $\alpha \gg \epsilon_r$, there is a range of time scales where one can neglect density fluctuations and describe the dynamics entirely in terms of $\Theta = \nabla\cdot\mathbf{w}$. One obtains again bacterial dots that display, however, polar structure.

APPENDIX C: LINEAR STABILITY OF THE POLARIZED STATE

To examine the linear stability of the polarized state, we linearize Eqs. (1) of this paper in fluctuations about a uniform polar state by letting

$$\delta\tilde{\rho}(\mathbf{r},t) = \tilde{\rho}(\mathbf{r},t) - 1 , \quad \text{(C1)}$$

$$\delta\tilde{\mathbf{w}}(\mathbf{r},t) = \tilde{\mathbf{w}}(\mathbf{r},t) - \mathbf{w}_0/\rho_s , \quad \text{(C2)}$$

where $\mathbf{w}_0 = \hat{\mathbf{x}}w_0$ and $w_0 = \sqrt{2\epsilon(\gamma\rho_s - \epsilon)}/\gamma$. Since the polarized state exists for $\gamma\rho_s > \epsilon$, to simplify the notation below we introduce the dimensionless parameter $\eta = \gamma w_0/\epsilon = \sqrt{2(\gamma\rho_s - \epsilon)/\epsilon}$, which is positive in the polar state and vanishes at the mean-field transition. The linearized equations are then given by

$$\partial_t\delta\tilde{\rho} = -v\nabla\cdot\delta\tilde{\mathbf{w}} - \frac{\epsilon\eta}{\gamma}v'\partial_x\delta\tilde{\rho} + D\nabla^2\delta\tilde{\rho} - \alpha\delta\tilde{\rho} , \quad \text{(C3a)}$$

$$\partial_t\delta\tilde{\mathbf{w}} = -\epsilon\eta^2\delta\tilde{w}_x\hat{\mathbf{x}} + \epsilon\eta\delta\tilde{\rho}\hat{\mathbf{x}} - \frac{1}{2} \times\left[(v + \rho_s v')\nabla - \frac{3}{4}\frac{\epsilon\eta^2}{\gamma}v'\nabla + \frac{\epsilon\eta^2}{4\gamma}v'\hat{\mathbf{x}}\partial_x\right]\delta\tilde{\rho} + \frac{3}{4}\eta v\nabla\delta\tilde{w}_x - \frac{1}{8}\eta v\partial_x\delta\tilde{\mathbf{w}} + D\nabla^2\delta\tilde{\mathbf{w}} . \quad \text{(C3b)}$$

Introducing spatial Fourier transforms $(\delta\tilde{\rho},\delta\tilde{\mathbf{w}}) = \Sigma_{\boldsymbol{q}}(\rho_{\boldsymbol{q}},\mathbf{w}_{\boldsymbol{q}})e^{i\boldsymbol{q}\cdot\boldsymbol{r}}$, the equations for the Fourier amplitudes are given by

$$\partial_t\rho_{\boldsymbol{q}} = -vi\mathbf{q}\cdot\mathbf{w}_{\mathbf{q}} - \frac{\epsilon\eta}{\gamma}v'iq_x\rho_{\boldsymbol{q}} - Dq^2\delta\tilde{\rho} - \alpha\rho_{\boldsymbol{q}} , \quad \text{(C4a)}$$

$$\partial_t\mathbf{w}_{\mathbf{q}} = -\epsilon\eta^2 w_{\mathbf{q}}^x\hat{\mathbf{x}} + \epsilon\eta\rho_{\mathbf{q}}\hat{\mathbf{x}} - \frac{1}{2} \times\left[(v + \rho_s v')i\mathbf{q} - \frac{3}{4}\frac{\epsilon\eta^2}{\gamma}v'i\mathbf{q} + \frac{\epsilon\eta^2}{4\gamma}v'\hat{\mathbf{x}}iq_x\right]\rho_{\boldsymbol{q}} + \frac{3}{4}\eta vi\mathbf{q}w_{\mathbf{q}}^x - \frac{1}{8}\eta viq_x\mathbf{w}_{\mathbf{q}} - Dq^2\mathbf{w}_{\mathbf{q}} . \quad \text{(C4b)}$$

For finite α, the dispersion relations of all the modes are finite at $q = 0$. A proper analysis of the linear stability of the

fluctuations then requires examining the modes up to order q^4. This is cumbersome and not very enlightening. For this reason we simply present here the analysis of the case $\lambda = 0$ and $\alpha = 0$ that serves to make contact with the existing literature.

1. Linear modes for $\alpha = 0$ and $\lambda = 0$

It is convenient to apportion the polarization in components along the direction $\hat{\mathbf{x}}$ of mean order and perpendicular to it. In addition, for simplicity we only consider wave vectors $\mathbf{q}$ along these two special directions.

2. Linear modes for $\mathbf{q} = q\hat{\mathbf{x}}$.

When $\mathbf{q} = q\hat{\mathbf{x}}$, $w^x_{\mathbf{q}}$ and $w^y_{\mathbf{q}}$ describe splay and bend deformations of the order parameter, respectively. The linearized equations are given by

$$\partial_t \rho_{\boldsymbol{q}} = -iqvw^x_{\mathbf{q}} - Dq^2\rho_{\boldsymbol{q}} \,, \tag{C5a}$$

$$\partial_t w^x_{\mathbf{q}} = -\epsilon\eta^2 w^x_{\mathbf{q}} + \epsilon\eta\rho_{\mathbf{q}} - \tfrac{1}{2}iqv\rho_{\mathbf{q}} + \tfrac{5}{8}\eta viqw^x_{\mathbf{q}} - Dq^2 w^x_{\mathbf{q}} \,, \tag{C5b}$$

$$\partial_t w^y_{\mathbf{q}} = -\tfrac{1}{8}\eta viqw^y_{\mathbf{q}} - Dq^2 w^y_{\mathbf{q}} \,. \tag{C5c}$$

Bend fluctuations are decoupled and always stable. The decay of coupled density and splay fluctuations is governed by modes with dispersion relation $s_\pm(q)$:

$$s_\pm(q) = \tfrac{1}{2}\big(-\epsilon\eta^2 + \tfrac{5}{8}\eta viq - 2Dq^2\big) \pm \tfrac{1}{2}\sqrt{\big(\epsilon\eta^2 - \tfrac{5}{8}\eta viq\big)^2 - 4iqv\big(\epsilon\eta - \tfrac{1}{2}iqv\big)} \tag{C6}$$

Notice that in the limit $\alpha = 0$, $s_-(0) = -\epsilon\eta^2$, which is nonhydrodynamic and hence ignored. The linear stability of the longitudinal mode to splay fluctuations is then determined by the hydrodynamic mode $s_+(q)$, and it is sufficient to expand it to second order in q:

$$s_+(q) = -\frac{ivq}{\eta} + \left(-D + \frac{v^2}{\epsilon\eta^4} + \frac{v^2}{8\epsilon\eta^2}\right)q^2 + O(q^4) \,. \tag{C7}$$

The system is unstable when $\mathrm{Re}[s_+] > 0$. When $D \to 0$, this condition is always satisfied. A finite D sets an upper limit for the instability

$$1 < \gamma\rho_s < \frac{v}{4}\sqrt{\frac{\epsilon}{D}} \,. \tag{C8}$$

Notice that the mode $s_+(q)$ has a finite imaginary part, which suggests the emergence traveling patterns in the unstable region. This longitudinal instability of splay and density fluctuations is simply the banding instability studied by Bertin *et al.* [29] and by Mishra *et al.* [30], although the parameters in our model have a different dependence on v_0, in particular, the alignment parameter γ does not depend on v_0.

3. Linear modes for $\mathbf{q} = q\hat{\mathbf{y}}$.

If $\mathbf{q} = q\hat{\mathbf{y}}$, $\alpha = 0$, and $\lambda = 0$, then the linearized equations for the fluctuations are given by

$$\partial_t \rho_{\mathbf{q}} = -viqw^y_{\mathbf{q}} - Dq^2\rho_{\mathbf{q}} \,, \tag{C9a}$$

$$\partial_t w^x_{\mathbf{q}} = -\epsilon\eta^2 w^x_{\mathbf{q}} + \epsilon\eta\rho_{\mathbf{q}} - Dq^2 w^x_{\mathbf{q}} \,, \tag{C9b}$$

$$\partial_t w^y_{\mathbf{q}} = -\tfrac{1}{2}viq\rho_{\mathbf{q}} + \tfrac{3}{4}v\eta iqw^x_{\mathbf{q}} - Dq^2 w^y_{\mathbf{q}} \,. \tag{C9c}$$

We first consider the region $\epsilon\eta \gg 1$, deep in the ordered state. In this case we can eliminate $w^x_{\mathbf{q}}$ by neglecting the time derivative in Eq. (C9b) to obtain

$$w^x_{\mathbf{q}} \simeq \frac{1}{\eta}\rho_{\mathbf{q}}. \tag{C10}$$

Substituting in Eqs. (C9a) and (C9c), we obtain coupled equations for density and bend fluctuations, given by

$$\partial_t \rho_{\mathbf{q}} = -viqw^y_{\mathbf{q}} - Dq^2\rho_{\mathbf{q}} \,, \tag{C11a}$$

$$\partial_t w^y_{\mathbf{q}} = \tfrac{1}{4}viq\rho_{\mathbf{q}} - Dq^2 w^y_{\mathbf{q}}. \tag{C11b}$$

The dispersion relations $s_\pm(q)$ of the eigenvalues of these equations are given by

$$s_\pm(q) = \pm\frac{vq}{2} - \frac{Dq^2}{2}. \tag{C12}$$

We see that $\mathrm{Re}[s_-]$ is always negative. The linear stability of the polarized state to fluctuations with the wave vector along y is determined by the s_+ mode, which is always unstable for $0 < q < \frac{v}{2D}$. Therefore deep in the ordered region, the polarized state is always unstable to bend fluctuations. This arises from the pressurelike term proportional to the w^2 term that yields a change in sign of the effective compressibility, as discussed in Ref. [30].

APPENDIX D: EFFECT OF ADDITIONAL NONLINEAR ADVECTIVE TERMS

The continuum model considered in this article is a simplified version of the model obtained in Ref. [24] by coarse graining a microscopic Vicsek model with a density-dependent self-propulsion speed. In Eqs. (1) of the paper we have neglected a number of additional advective nonlinearities that are obtained from the exact coarse graining. In this section we show that these additional nonlinear terms do not change the nature of the patterns but simply yield small shifts in the values of parameters where each type of pattern is obtained.

Farrell *et al.* [24] considered a Vicsek-type model of point particles with density-dependent self-propulsion speed $v(\rho)$. The microscopic dynamics is governed by coupled Langevin equations of the form

$$\dot{\mathbf{r}}_i = v\hat{\mathbf{e}}_i + \boldsymbol{\eta}_i(t) \,, \tag{D1a}$$

$$\dot{\theta}_i = -\gamma\frac{\partial U}{\partial\theta_i} + \eta^R_i(t), \tag{D1b}$$

where $v(\rho) = v_0\exp(-\lambda\rho)$, $\mathbf{r}_i$ is the position of the active particle, and $\hat{\mathbf{e}}_i$ a unit vector along the direction of self-propulsion. The microscopic dynamics includes white and Gaussian thermal and rotational noise terms, with correlations

$$\langle\eta_{i\alpha}(t)\eta_{j\beta}(t')\rangle = 2D\delta_{ij}\delta_{\alpha\beta}\delta(t-t') \,, \tag{D2}$$

$$\left\langle\eta^R_i(t)\eta^R_j(t')\right\rangle = 2\epsilon\delta_{ij}\delta(t-t') \,. \tag{D3}$$

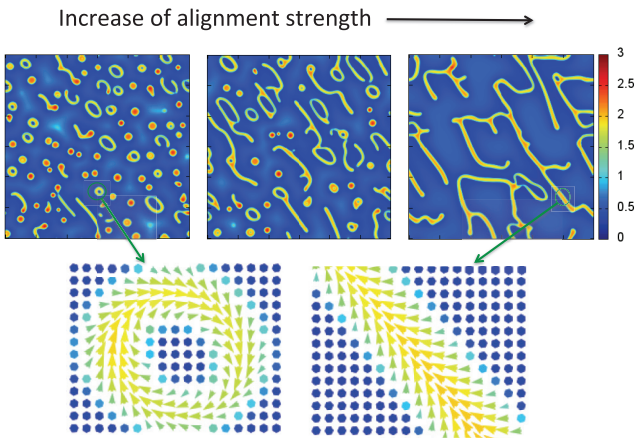

FIG. 7. (Color online) Heat maps of density in the polar region obtained by numerical integration of Eqs. (D4) for $\tilde{\lambda} = 1.4, \tilde{\alpha} = 0.08$, and $\tilde{D} = 0.01$ and (from left to right) $\tilde{\gamma} = 1.11, 1.25$, and 1.67.

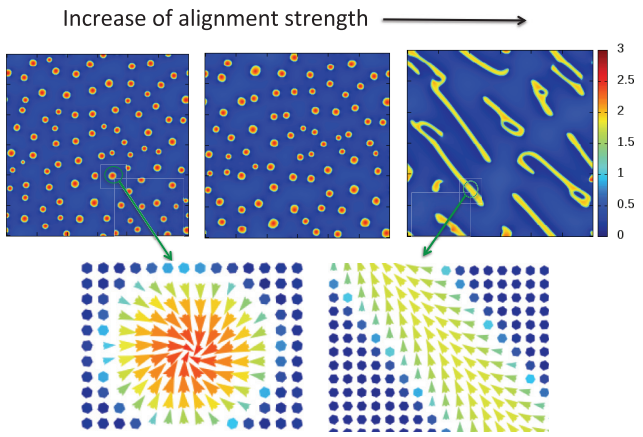

FIG. 8. (Color online) Heat maps of density in the polar region obtained by numerical integration of the simplified equations, Eqs. (1) of the paper for $\tilde{\lambda} = 1.4, \tilde{\alpha} = 0.08$, $\tilde{D} = 0.01$ and (from left to right) $\tilde{\gamma} = 1.11, 1.25$, and 1.67.

Finally, $U = -\sum_{|\mathbf{r}_j - \mathbf{r}_i| \leqslant R} \cos(\theta_j - \theta_i)$ is the polar alignment interaction. Using standard coarse graining, these authors derived continuum equations for density and polarization, given by (with our parameter notation)

$$\partial_t \rho = -\nabla \cdot (v\mathbf{w} - D\nabla\rho) + \alpha\rho(1 - \rho/\rho_s)\,, \qquad \text{(D4a)}$$

$$\partial_t \mathbf{w} = -(\epsilon - \gamma\rho)\mathbf{w} - \frac{\gamma^2}{2\epsilon}|\mathbf{w}|^2\mathbf{w} - \frac{\gamma}{4\epsilon}\mathbf{F}[\mathbf{w}, \nabla\mathbf{w}] - \frac{1}{2}\nabla\left(v\rho - \frac{3\gamma}{4\epsilon}vw^2\right) + D_w\nabla^2\mathbf{w}\,. \qquad \text{(D4b)}$$

Compared to the simplified model described by Eqs. (1) in the paper, Eqs. (D4) contain a more complicated form for the advective nonlinearities $\mathbf{F}[\mathbf{w}, \nabla\mathbf{w}]$, given by $\mathbf{F} = \frac{1}{2}\mathbf{w}\cdot\nabla(v\mathbf{w}) + \frac{1}{4}v\nabla w^2 + \frac{3}{2}\mathbf{w}\nabla\cdot(v\mathbf{w}) + v\mathbf{w}(\nabla\cdot\mathbf{w}) + v(\mathbf{w}\cdot\nabla)\mathbf{w}$ (only the first term is included in Eqs. (1) of the paper). These additional terms have, however, little effect on the nature of the emergent patterns, but only shift the parameters where the patterns emerge, as illustrated by Figs. 7 and 8. The only exception is that the full form of $\mathbf{F}[\mathbf{w}, \nabla\mathbf{w}]$ must be included to obtain the blinking dots shown in Supplementary Movie 5 in the isotropic state [34].

[1] J. D. Murray, *Mathematical Biology, Spatial Models and Biomedical Applications*, Vol. II, 3rd ed. (Springer, New York, 2003).
[2] E. O. Budrene and H. Berg, Nature (London) **376**, 49 (1995).
[3] D. Woodward, R. Tyson, M. R. Myerscough, J. D. Murray, E. O. Budrene, and H.C. Berg, Biophys. J. **68**, 2181 (1995).
[4] V. Schaller, C. Weber, C. Semmrich, E. Frey, and A. R. Bausch, Nature (London) **467**, 73 (2010).
[5] T. Butt, T. Mufti, A. Humayun, P. B. Rosenthal, S. Khan, S. Khan, and J. E. Molloy, J. Biol. Chem. **285**, 4964 (2010).
[6] F. Nédélec, T. Surrey, A. Maggs, and S. Leibler, Nature (London) **389**, 305 (1997).
[7] T. Surrey, F. J. Nédélec, S. Leibler, and E. Karsenti, Science **292**, 1167 (2001).
[8] C. Liu, X. Fu, L. Liu, X. Ren, C. K. L. Chau, S. Li, L. Xiang, H. Zeng, G. Chen, L.-H. Tang *et al.*, Science **334**, 238 (2011).
[9] R. Thar and M. Kühl, FEMS Microbiol. Lett. **246**, 75 (2005).
[10] K. Doubrovinski and K. Kruse, Europhys. Lett. **83**, 18003 (2008).
[11] K. Doubrovinski and K. Kruse, Phys. Rev. Lett. **107**, 258103 (2011).
[12] A. E. Carlsson, Phys. Rev. Lett. **104**, 228102 (2010).
[13] M. G. Vicker, Exp. Cell Res. **275**, 54 (2002).
[14] S. Whitelam, T. Bretschneider, and N. J. Burroughs, Phys. Rev. Lett. **102**, 198103 (2009).
[15] E. Ben-Jacob, I. Cohen, and H. Levine, Adv. Phys. **49**, 395 (2000).
[16] M. P. Brenner, Proc. Nat. Acad. Sci. USA **107**, 11653 (2010).
[17] J. Tailleur and M. E. Cates, Phys. Rev. Lett. **100**, 218103 (2008).
[18] M. E. Cates, D. Marenduzzo, I. Pagonabarraga, and J. Tailleur, PNAS **107**, 11715 (2010).
[19] J. Toner, Phys. Rev. Lett. **108**, 088102 (2012).
[20] X. Fu, L.-H. Tang, C. Liu, J.-D. Huang, T. Hwa, and P. Lenz, Phys. Rev. Lett. **108**, 198102 (2012).
[21] J. Toner and Y. Tu, Phys. Rev. Lett. **75**, 4326 (1995).
[22] J. Toner, Y. Tu, and S. Ramaswamy, Ann. Phys. **318**, 170 (2005).
[23] M. G. Forest, Q. Wang, and R. Zhou, Soft Matter **9**, 5207 (2013).
[24] F. Farrell, M. C. Marchetti, D. Marenduzzo, and J. Tailleur, Phys. Rev. Lett. **108**, 248101 (2012).
[25] Y. Fily, A. Baskaran, and M. C. Marchetti, Soft Matter **8**, 3002 (2012).
[26] G. S. Redner, M. F. Hagan, and A. Baskaran, Phys. Rev. Lett. **110**, 055701 (2013).
[27] N. Mittal, E. O. Budrene, M. P. Brenner, and A. van Oudenaarden, Proc. Nat. Acad. Sci. USA **100**, 13259 (2003).
[28] See Fig. 5 of Ref. [27], and associated discussion.

[29] E. Bertin, M. Droz, and G. Grégoire, J. Phys. A: Math. Theor. **42**, 445001 (2009).

[30] S. Mishra, A. Baskaran, and M. C. Marchetti, Phys. Rev. E **81**, 061916 (2010).

[31] T. Bretschneider, K. Anderson, M. Ecke, A. Müller-Taubenberger, B. Schroth-Diez, H. C. Ishikawa-Ankerhold, and G. Gerisch, Biophys. J. **96**, 2888 (2009).

[32] This is estimated as the rotational diffusion of an F-actin cylinder of length 1 μm and thickness 5 nm, in a medium of viscosity $\eta = 1 - 10$ cP, appropriate for water and the cytosol, respectively: see, e.g., M. Doi and S. F. Edwards, *The Theory of Polymer Dynamics* (Oxford Science Publications, Oxford, UK, 1986).

[33] E. Lushi, R. E. Goldstein, and M. J. Shelley, Phys. Rev. E **86**, 040902(R) (2012).

[34] See Supplemental Material at http://link.aps.org/supplemental/10.1103/PhysRevE.89.012711 for movies of the patterns and their evolution for a number of parameter choices.